X-ray Absorption Spectra of Nickel Complexes with N_3S_2 Chromophores and Spectroscopic Studies on H^- and CO Binding at These Nickel Centers: Relevance to the Reactivity of the Nickel Site(s) in [FeNi] Hydrogenases

Narayan Baidya,[†] Marilyn M. Olmstead,[‡] Joyce P. Whitehead,[§] Csaba Bagyinka,[§] Michael J. Maroney,[§] and Pradip K. Mascharak*[,†]

Department of Chemistry and Biochemistry, Thimann Laboratories, University of California, Santa Cruz, California 95064, Department of Chemistry, University of California, Davis, California 95616, and Department of Chemistry and Program in Molecular and Cellular Biology, University of Massachusetts, Amherst, Massachusetts 01003

Received April 21, 1992

The reaction of $[Ni(terpy)Cl_2]$ with ~2.0 equiv of 2,6-$(Me)_2C_6H_3S^-$ in acetonitrile affords the distorted trigonal bipyramidal (tbp) complex $[Ni(terpy)(2,6\text{-}(Me)_2C_6H_3S)_2]$ (**4**). Complex **4** crystallizes in the orthorhombic space group *Pbcn* with $a = 21.881$ (7) Å, $b = 11.461$ (3) Å, $c = 10.557$ (3) Å, $V = 2647.4$ (13) Å^3, and $Z = 4$. The structure of **4** was refined to $R = 4.31\%$ on the basis of 1673 ($F > 4\sigma(F)$) data. Comparisons of the results of X-ray absorption spectroscopy (XAS) for complex **4** as well as $[Ni(terpy)(2,4,6\text{-}(i\text{-}Pr)_3C_6H_2S)_2]$ (**3**) and $[Ni(terpy)(C_6F_5S)_2]$ (A) (desolvated $[Ni(terpy)(C_6F_5S)_2(CH_3CN)]$ (**2**)) with those for the [FeNi] hydrogenase from *Thiocapsa roseopersicina* indicate that the nickel center in the enzyme is in a distorted tbp geometry with a mixed N/O- and S-donor environment. In this regard, complexes **3**, **4**, and **2** (without the acetonitrile molecule) are good structural models for the biological nickel site. In solvents like acetonitrile and DMSO, complex **2** generates hexacoordinated solvent adducts whose XAS data are quite different from those of the parent complex A as well as **3** and **4**. X-ray absorption near-edge spectroscopy (XANES) shows a weaker 1s → 3d transition for these hexacoordinated adducts compared to the parent complex A. EXAFS features of the solvated hexacoordinated adducts (maximum at $k = 4$ Å^{-1}) are also different from the EXAFS data for the pentacoordinated complexes (maximum at $k = 6$ Å^{-1}). The model complexes **2**–**4** are readily reduced to the corresponding Ni(I) species with reductants like $Na_2S_2O_4$ in DMF. The EPR spectra of the reduced complexes as well as the substrate (CO, H^-, and R^-)-bound Ni(I) species have been discussed. Close similarities between the EPR spectra of the hydride adducts of reduced **3** and **4** and the Ni-C signal of the hydrogenase from *T. roseopersicina* support the formalism Ni(I)–H^- for the nickel site in form C of the enzyme.

Introduction

In several microorganisms, the reversible oxidation of hydrogen is catalyzed by the enzyme hydrogenase.[1-5] According to the cofactor present, these enzymes are divided into three main groups: (i) Fe-only hydrogenase, (ii) [FeNi] hydrogenase, and (iii) [FeNiSe] hydrogenase.[1] The active site of [FeNi] hydrogenases contains 1 equiv of nickel in addition to Fe–S clusters.[1] EPR studies on different [FeNi] hydrogenases indicate that the nickel center or centers in these enzymes serve as the binding sites for the substrate hydrogen.[6] Carbon monoxide, an inhibitor of the enzyme, also binds at the nickel center reversibly.[6] Recent spectroscopic studies have indicated that the nickel center in [FeNi] hydrogenase from *Thiocapsa roseopersicina* exists in a distorted pentacoordinated geometry with three nitrogen/oxygen and two sulfur atoms in its first coordination sphere.[7] In order to elucidate the coordination structure of the nickel site in the enzyme, we initiated a synthetic analogue approach[8] that involves syntheses of nickel complexes with N_3S_2 chromophores. In such attempts, we utilize 2,6′:2′,6″-terpyridine (terpy) and aromatic thiolates as sources for the three nitrogen and two sulfur atoms around the nickel center (reaction I).[9] Reaction of $[Ni(terpy)Cl_2]$ with thiophenolate, $C_6H_5S^-$, affords the thiolato-bridged dimeric complex $[Ni(terpy)(C_6H_5S)_2]_2$ (**1**), while, with the less basic pentafluorothiophenolate, $C_6F_5S^-$, the hexacoordinated

[†] University of California, Santa Cruz.
[‡] University of California, Davis.
[§] University of Massachusetts.

(1) (a) Moura, J. J. G.; Moura, I.; Teixeira, M.; Xavier, A. V.; Fauque, G. D.; LeGall, J. *Met. Ions. Biol. Syst.* **1988**, *23*, 285. (b) Moura, J. J. G.; Teixeira, M.; Moura, I.; LeGall, J. In *The Bioinorganic Chemistry of Nickel*; Lancaster, J. R., Jr., Ed.; VCH Publishers: Deerfield Beach, FL, 1988; Chapter 9, p 191. (c) Bastian, N. R.; Wink, D. A.; Wackett, L. P.; Livingston, D. J.; Jordon, L. M.; Fox, J.; Orme-Johnson, W. H.; Walsh, C. T. In *The Bioinorganic Chemistry of Nickel*; Lancaster, J. R., Jr., Ed.; VCH Publishers: Deerfield Beach, FL, 1988; Chapter 10, p 227. (d) Moura, J. J. G.; Teixeira, M.; Moura, I.; Xavier, A. V.; LeGall, J. In *Frontiers of Bioinorganic Chemistry*; Xavier, A. V., Ed.; VCH Publishers: Deerfield Beach, FL, 1986; p 3. (e) Moura, J. J. G.; Teixeira, M.; Moura, I. *J. Mol. Catal.* **1984**, *23*, 303.
(2) (a) Cammack, R. *Adv. Inorg. Chem.* **1988**, *32*, 297. (b) Albracht, S. P. J.; van der Zwaan, J. W.; Fontijn, R. D.; Slater, E. C. In *Frontiers of Bioinorganic Chemistry*; Xavier, A. V., ed; VCH Publishers: Deerfield Beach, FL, 1986; p 11. (c) Cammack, R.; Hall, D. O.; Rao, K. K. In *Gas Metabolism: Mechanistic, Metabolic and Biotechnological Aspects*; Poole, R. K., Dow, C. S., Eds.; Academic Press: New York, 1985.
(3) (a) Hausinger, R. P. *Microbiol. Rev.* **1987**, *51*, 22. (b) Walsh, C. T.; Orme-Johnson, W. H. *Biochemistry* **1987**, *26*, 4901.
(4) (a) Fauque, G.; Peck, H. D., Jr.; Moura, J. J. G.; Huynh, B. H.; Berlier, Y.; DerVartanian, D. V.; Teixeira, M.; Przybyla, A. E.; Lespinat, P. A.; Moura, I.; LeGall, J. *FEMS Microbiol. Rev.* **1988**, *54*, 299. (b) Vignais, P. M.; Colbeau, A.; Willison, J. C.; Jouanneau, Y. *Adv. Microb. Physiol.* **1985**, *26*, 155.
(5) Adams, M. W. W.; Mortenson, L. E.; Chen, J.-S. *Biochim. Biophys. Acta* **1980**, *594*, 105.
(6) (a) van der Zwaan, J. W.; Coremans, J. M. C. C.; Bouwens, E. C. M.; Albracht, S. P. J. *Biochim. Biophys. Acta* **1990**, *1041*, 101. (b) van der Zwaan, J. W.; Albracht, S. P. J.; Fontijn, R. D.; Roelofs, Y. B. M. *Biochim. Biophys. Acta* **1986**, *872*, 208. (c) van der Zwaan, J. W.; Albracht, S. P. J.; Fontijn, R. D.; Slater, E. C. *FEBS Lett.* **1985**, *179*, 271.
(7) (a) Maroney, M. J.; Colpas, G. J.; Bagyinka, C.; Baidya, N.; Mascharak, P. K. *J. Am. Chem. Soc.* **1991**, *113*, 3962. (b) Colpas, G. J.; Maroney, M. J.; Bagyinka, C.; Kumar, M.; Willis, W. S.; Suib, S. L.; Baidya, N.; Mascharak, P. K. *Inorg. Chem.* **1991**, *30*, 920. (c) Maroney, M. J.; Colpas, G. J.; Bagyinka, C. *J. Am. Chem. Soc.* **1990**, *112*, 7067.
(8) Ibers, J. A.; Holm, R. H. *Science (Washington, D.C.)* **1980**, *209*, 223.
(9) Baidya, N.; Olmstead, M.; Mascharak, P. K. *Inorg. Chem.* **1991**, *30*, 929.

0020-1669/92/1331-3612$03.00/0 © 1992 American Chemical Society

$$[Ni(terpy)Cl_2] + 2RS^- \longrightarrow (1\text{-}4) \qquad (I)$$

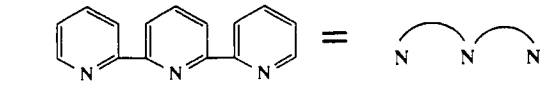

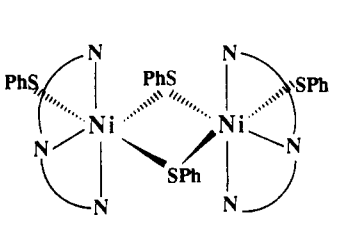

(1)

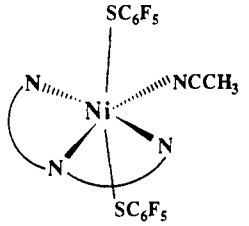

(2)

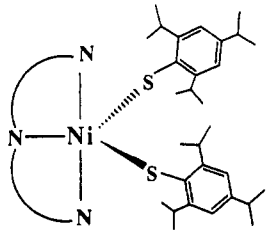

(3)

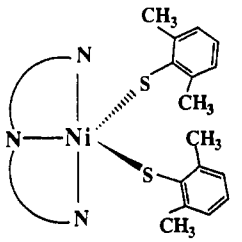

(4)

species $[Ni(terpy)(C_6F_5S)_2(CH_3CN)]$ (**2**) is isolated, in which the sixth site on nickel is occupied by a solvent (acetonitrile) molecule. The first example of the desired mononuclear pentacoordinated complex with an N_3S_2 chromophore has been obtained with 2,4,6-triisopropylthiophenolate (2,4,6-$(i\text{-}Pr)_3C_6H_2S^-$) as the complex $[Ni(terpy)(2,4,6\text{-}(i\text{-}Pr)_3C_6H_2S)_2]$ (**3**). The steric bulk of the isopropyl groups of the thiolate ligands prevents bridge formation and leaves just enough space for small ligands like CO and hydride (but not a solvent molecule) to coordinate to nickel in **3**. Successful isolation of **3** raised an interesting question regarding the minimum steric bulk necessary to achieve pentacoordination in this type of complex. Therefore, in our next attempt, we selected 2,6-dimethylthiophenolate (2,6-$(Me)_2C_6H_3S^-$), in which the isopropyl groups are substituted by methyl groups (the smallest possible alkyl group) on the benzene ring of the thiolate ligand. The structure and properties of $[Ni(terpy)(2,6\text{-}(Me)_2C_6H_3S)_2]$ (**4**) are reported in this paper. Also reported are the results of X-ray absorption spectroscopy (XAS) for **2**–**4**. A comparison of the model data with those for the hydrogenase from *T. roseopersicina* confirms that complexes **3** and **4** (and **2** without the coordinated acetonitrile molecule) are good structural models of the nickel site in the enzyme. Results of ligand-binding studies for **3** and **4** have been compared with those for the enzyme in order to explore the oxidation state and configuration(s) of the nickel center in the Ni–C species, the active intermediate formed during the catalytic cycle of hydrogenases.[2b] Striking similarities between the EPR spectra of the H^- adducts of complexes **3** and **4** in the reduced state and Ni–C signal of hydrogenase from *T. roseopersicina* support the presence of Ni(I) in the Ni–C state of the enzyme.[2b]

Experimental Section

2,6-Dimethylbenzenethiol was procured from Aldrich Chemical Co. and was used without further purification. $[Ni(terpy)Cl_2]$ was synthesized by following a published procedure.[10] In the following preparations, degassed solvents were used and all manipulations were performed under an atmosphere of dry and pure dinitrogen.

$[Ni(terpy)(2,6\text{-}(Me)_2C_6H_3S)_2]$ (4). A solution of (Me_4N^+)-$(2,6\text{-}(Me)_2C_6H_3S^-)$ prepared from 140 mg of $2,6\text{-}(Me)_2C_6H_3SH$ and 181 mg of $(Me_4N)OH\cdot 5H_2O$ in 25 mL of acetonitrile was slowly added to a suspension of $[Ni(terpy)Cl_2]$ in 25 mL of the same solvent. The resulting dark brown solution was stirred for 2 h, during which red microcrystals separated. These were collected by filtration and dried under vacuum. Crystals used in the X-ray work were obtained by slow cooling of the filtrate from this step. The combined yield was 180 mg (70%). Anal. Calcd for $C_{31}H_{29}N_3S_2Ni$: C, 65.74; H, 5.16; N, 7.42. Found: C, 65.52; H, 5.01; N, 7.23. Selected IR bands (KBr pellet, cm^{-1}): 2938 (m), 1598 (s), 1560 (m), 1450 (s), 1421 (m), 1162 (m), 1055 (s), 1012 (m), 828 (w), 774 (s), 761 (s), 733 (m), 634 (w). ^1H NMR (300 MHz, $(CD_3)_2SO$, 298 K), δ (ppm from TMS)): 176.68 (2 H), 79.23 (2 H), 73.43 (2 H), 50.98 (2 H), 22.63 (4 H), 21.02 (1 H), 18.69 (14 H), −21.95 (2 H).

Sample Preparation. *T. roseopersicina* hydrogenase was isolated and purified by following a published procedure.[7a] The enzyme activity was monitored by gas chromatographic quantitation of H_2 production in the presence of reduced methyl viologen,[11] while the protein concentration was determined by using the absorbance at 220 nm with bovine serum albumin as the standard. For XAS measurements, the enzyme sample was prepared in 20 mM Tris-HCl buffer (pH 8) that also contained 20% glycerol. The final nickel concentration was 0.28 mM. The enzyme was first fully reduced by exposure to H_2 overnight (no EPR signal) and was then oxidized back to form C (EPR active, $S = {}^1/_2$ spectrum) with the aid of oxidized benzyl viologen. Integration of the EPR signal at 120 K indicated a concentration of 0.96 spin/protein.

No significant difference in activity was detected in the sample before and after exposure to synchrotron radiation.

XAS Data Collection and Analysis. Ni K-edge X-ray absorption data were collected on beam line X-9A at the National Synchrotron Light Source (NSLS) of Brookhaven National Laboratory under dedicated conditions (2.53 GeV, 60–120 mA). The Si(111) double crystal monochromator was calibrated against the first inflection point of nickel foil (8331.6 eV) and provided a theoretical resolution of ca. 1 eV at 8.3 keV for a 1-mm hutch slit height. Edge energy calibrations were reproducible to within ±0.2–0.3 eV. Harmonic rejection was accomplished by keeping a focusing mirror flat. Both external and internal edge energy calibration methods were used.

Data for the model compounds were collected in the transmission mode on powdered samples diluted with boron nitride to reduce thickness effects. Nitrogen (I_0) and argon (I) filled ionization chambers were used. Spectra were run at room temperature with the samples kept under He atmosphere. At least two spectra were run for each sample to check for reproducibility.

Fluorescence data were collected on frozen solutions with use of a 13-element Ge detector. The samples were held in thermal contact with liquid N_2 in an evacuated cryostat. For the protein, the reported spectra are the weighted sums of the data obtained from each element for 20 scans by using the procedure described by Scott,[12] while, for the model complexes, two scans were run for each sample.

The edge regions of the XAS spectra were analyzed by the procedure described in our earlier account.[7b] Details of procedures for EXAFS data analysis have also been reported previously by this group.[7a]

X-ray Data Collection and Structure Solution and Refinement. Dark needles of **4** were obtained by slowly cooling a solution of the complex in acetonitrile. Diffraction experiments were performed at 130 K on a Syntex $P2_1$ machine equipped with graphite monochromator and modified LT-1 low-temperature apparatus. Mo Kα radiation (λ = 0.710 69 Å) was employed. Intensities of two standard reflections showed only random fluctuations of less than 2% during the course of data collection. The structure of **4** was solved by direct methods.[13,14] Hydrogen atoms bonded to the carbon atoms were included at calculated positions by using a

(10) Judge, J. S.; Reiff, W. M.; Intille, G. M.; Ballway, P.; Baker, W. A. *J. Inorg. Nucl. Chem.* **1967**, *29*, 1711.
(11) Bagyinka, C.; Zorin, N. A.; Kovacs, K. L. *Anal. Biochem.* **1984**, *142*, 7.
(12) Scott, R. A. *Methods Enzymol.* **1985**, *117*, 414.
(13) Siemens SHELXTL PLUS (VMS) installed on a Micro VAX 3200 computer.
(14) Neutral-atom scattering factors were taken from: *International Tables for X-ray Crystallography*; Kynoch Press: Birmingham, England, 1974; Vol. IV.

Table I. Summary of Crystal Data and Intensity Collection and Structure Refinement Parameters for [Ni(terpy)(2,6-$(Me)_2C_6H_3S)_2$] (**4**)

formula (mol wt)	$C_{31}H_{29}N_3S_2Ni$ (566.41)
color and habit	dark needles
cryst syst	orthorhombic
space group	*Pbcn*
a, Å	21.881 (7)
b, Å	11.461 (3)
c, Å	10.557 (3)
V, Å^3	2647.4 (13)
Z	4
cryst dimens, mm	0.13 × 0.18 × 0.50
d_{calcd}(130 K), g cm^3	1.421
μ(Mo Kα), cm^{-1}	9.12
transm coeff	0.87–0.91
scan method	ω, 1.0° range
2θ range, deg	0–50
no. of data collected	2676
no. of data used in refinement	1673 [$F > 4.0\sigma(F)$]
no. of params refined	169
R^a	4.31
$R_w{}^b$	3.89 [$w^{-1} = \sigma^2(F) + 0.0002F^2$]
GOF	1.18
largest Δ/σ	0.001
largest difference peak, e Å^{-3}	0.38

^{a} $R = \sum||F_o| - |F_c||/|F_o|$. ^{b} $R_w = \sum||F_o| - |F_c||w^{1/2}/\sum|F_o w^{1/2}|$.

Table II. Atomic Coordinates (×10^4) and Equivalent Isotropic Displacement Coefficients (Å^2 × 10^3) for [Ni(terpy)(2,6-$(Me)_2C_6H_3S)_2$] (**4**)

	x	*y*	*z*	*U*(eq)^a
Ni	0	2619 (1)	2500	15 (1)
S	773 (1)	1849 (1)	1264 (1)	23 (1)
N(1)	550 (1)	2997 (3)	4092 (3)	16 (1)
N(2)	0	4342 (3)	2500	15 (1)
C(1)	1377 (2)	1377 (3)	2267 (3)	19 (1)
C(2)	1331 (2)	310 (3)	2930 (4)	21 (1)
C(3)	1809 (2)	−44 (4)	3710 (4)	27 (1)
C(4)	2328 (2)	622 (4)	3838 (4)	27 (1)
C(5)	2370 (2)	1673 (4)	3205 (4)	26 (1)
C(6)	1904 (2)	2063 (3)	2422 (4)	20 (1)
C(7)	760 (2)	−415 (3)	2869 (4)	28 (1)
C(8)	1965 (2)	3213 (4)	1769 (4)	32 (2)
C(9)	845 (2)	2244 (3)	4848 (3)	18 (1)
C(10)	1288 (2)	2588 (4)	5715 (4)	25 (1)
C(11)	1415 (2)	3762 (4)	5836 (4)	27 (1)
C(12)	1099 (2)	4554 (4)	5099 (3)	23 (1)
C(13)	676 (2)	4153 (3)	4233 (3)	16 (1)
C(14)	336 (2)	4922 (3)	3358 (3)	14 (1)
C(15)	344 (2)	6138 (3)	3388 (4)	22 (1)
C(16)	0	6732 (4)	2500	19 (2)

^{a} Equivalent isotropic *U* defined as one-third of the trace of the orthogonalized U_{ij} tensor.

riding model, with C–H = 0.96 Å and $U_H = 1.2U_C$. The data were corrected for absorption effects by use of the program XABS.[15]

The structure of **4** was refined by full-matrix least-squares methods. Anisotropic thermal parameters were assigned to the non-hydrogen atoms in the final cycles of refinement. The largest feature on the final difference map was 0.38 e Å^{-3} in height. Machine parameters, crystal data, and data collection parameters are listed in Table I. Positional parameters are listed in Table II, while selected bond distances and angles are listed in Table III. The remaining crystallographic data have been submitted as supplementary material.

Other Physical Measurements. Infrared spectra were obtained with a Perkin-Elmer 1600 spectrophotometer. Absorption spectra were recorded on a Perkin-Elmer Lambda-9 spectrophotometer. ^{1}H NMR spectra were measured on a General Electric 300-MHz GN-300 instrument. A Johnson Matthey magnetic susceptibility balance was used to measure the room-temperature susceptibility value in the polycrystalline state. A Bruker ESP-300 spectrometer was used to record the EPR spectra at X-band frequencies.

(15) Moezzi, B. Ph.D. Dissertation, University of California, Davis, 1987. The program obtains an absorption tensor from the $F_o - F_c$ differences.

Table III. Bond lengths (Å) and Angles (deg) for [Ni(terpy)(2,6-$(Me)_2C_6H_3S)_2$] (**4**)^a

Bond Lengths			
Ni–S	2.311 (1)	Ni–N (1)	2.112 (3)
Ni–N(2)	1.975 (4)	S–C(1)	1.778 (4)
N(1)–C(9)	1.341 (5)	N(1)–C(13)	1.361 (5)
N(2)–C(14)	1.343 (4)	C(1)–C(2)	1.413 (5)
C(1)–C(6)	1.404 (5)	C(2)–C(3)	1.391 (6)
C(2)–C(7)	1.502 (5)	C(3)–C(4)	1.376 (6)
C(4)–C(5)	1.381 (6)	C(5)–C(6)	1.388 (5)
C(6)–C(8)	1.494 (6)	C(9)–C(10)	1.391 (5)
C(10)–C(11)	1.380 (6)	C(11)–C(12)	1.381 (6)
C(12)–C(13)	1.380 (5)	C(13)–C(14)	1.477 (5)
C(14)–C(15)	1.394 (5)	C(15)–C(16)	1.382 (5)
Bond Angles			
S–Ni–N(1)	96.4 (1)	S–Ni–N(2)	112.4 (1)
N(1)–Ni–N(2)	78.2 (1)	S–Ni–S′	135.1 (1)
N(1)–Ni–S′	92.6 (1)	N(2)–Ni–S′	112.4 (1)
S–Ni–N(1′)	92.6 (1)	N(1)–Ni–N(1′)	156.3 (2)
N(2)–Ni–N(1′)	78.2 (1)	Ni–S–C(1)	108.9 (1)
Ni–N(1)–C(9)	128.0 (3)	Ni–N(1)–C(13)	113.7 (2)
C(9)–N(1)–C(13)	117.6 (3)	Ni–N(2)–C(14)	119.7 (2)
C(14)–N(2)–C(14′)	120.7 (4)	S–C(1)–C(2)	120.4 (3)
S–C(1)–C(6)	120.6 (3)	C(2)–C(1)–C(6)	119.0 (3)
C(1)–C(2)–C(3)	119.5 (4)	C(1)–C(2)–C(7)	121.1 (3)
C(3)–C(2)–C(7)	119.3 (4)	C(2)–C(3)–C(4)	121.1 (4)
C(3)–C(4)–C(5)	119.5 (4)	C(4)–C(5)–C(6)	121.3 (4)
C(1)–C(6)–C(5)	119.6 (3)	C(1)–C(6)–C(8)	120.9 (3)
C(5)–C(6)–C(8)	119.5 (3)	N(1)–C(9)–C(10)	123.1 (4)
C(9)–C(10)–C(11)	118.5 (4)	C(10)–C(11)–C(12)	119.3 (4)
C(11)–C(12)–C(13)	119.3 (4)	N(1)–C(13)–C(12)	122.2 (3)
N(1)–C(13)–C(14)	114.2 (3)	C(12)–C(13)–C(14)	123.6 (4)
N(2)–C(14)–C(13)	113.7 (3)	N(2)–C(14)–C(15)	121.1 (3)
C(13)–C(14)–C(15)	125.2 (3)	C(14)–C(15)–C(16)	118.1 (4)
C(15)–C(16)–C(15′)	120.9 (5)		

^{a} Symmetry code: ′ = $-x, y, {}^1/_2 - z$.

Binding Studies. Binding studies included hydride, carbon monoxide, and alkyl groups as ligands. For EPR studies, DMF solutions were placed in quartz EPR tubes and reactions were performed in the temperature range 233–253 K. The reaction mixtures were frozen immediately for EPR measurements, which were recorded at 100 K. Typically, 0.5 mL of an ~5 mM solution of the compound was mixed with 0.5 equiv of $Na_2S_2O_4$ in 10 μL of H_2O to generate the reduced species. The carbon monoxide adducts of the reduced species were obtained by passing CO through solutions of the reduced complexes. The hydride adducts of the reduced species were produced by the addition of 1.0 equiv of $NaBH_4$ in 10 μL of ethanol. $NaBH_4$ served as the reductant in these reactions. When alkyllithium compounds in THF were used instead of $NaBH_4$, the alkyl adducts of the reduced species were obtained. The respective alkyl radicals were also observed in such reactions.

Results and Discussion

The reaction of [Ni(terpy)Cl_2] with 2,6-$(Me)_2C_6H_3S^-$ in acetonitrile affords the distorted trigonal bipyramidal complex [Ni(terpy)(2,6-$(Me)_2C_6H_3S)_2$] (**4**, Figure 1). The steric bulk of the methyl groups on the phenyl rings bonded to the S atoms allows isolation of the monomeric complex **4**; the unsubstituted benzenethiolate affords the bridged dimer **1**.[9] The same synthetic strategy also allows isolation of complex **3**, in which isopropyl groups are present on the 2, 4, and 6 positions of the phenyl ring.[9]

Structure of [Ni(terpy)(2,6-$(Me)_2C_6H_3S)_2$] (4). A computed-generated drawing of the complex is shown in Figure 1, and selected bond distances and angles are listed in Table III. The coordination geometry around nickel is distorted trigonal bipyramidal. As expected, the two bulky thiolate ligands are coordinated in the equatorial plane. The central nitrogen of the terpy ligand is the third donor atom in this plane, while the other two nitrogens of terpy occupy the two axial positions.

The S–Ni–S angles in the distorted tbp complexes **3**[9] and **4** are 130.1 (1) and 135.1 (1)° (Table III), respectively, and deviate considerably from the ideal angle of 120° due to the steric hindrance imposed by the ortho substituents of the thiolate ligands. It is interesting to note that this angle is larger in **4** even though

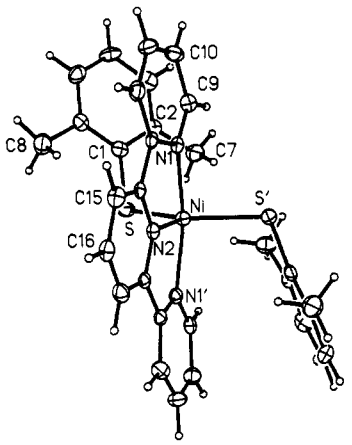

Figure 1. Computer-generated thermal ellipsoid (probability level 50%) plot of **4** with the atom-labeling scheme. Hydrogen atoms are given an arbitrary size.

the substituents on the thiolate ligands in the equatorial plane of **4** are less bulky (Me vs *i*-Pr in **3**). Close inspection of the two structures reveals that, in **3**, steric interactions between individual *i*-Pr groups of the thiolate ligands and the terpy moiety force the thiolate ligands away from the terpy framework.[9] This results in a compression of the S–Ni–S angle in the equatorial plane. In the case of **4**, this interaction is less significant and hence a slight increase (5°) in the S–Ni–S angle is observed (Figure 1). The terpy ligand framework is strictly planar (see Figure S1, supplementary material). The Ni(II)–S and Ni(II)–N distances (2.311 (1) and 2.044 (4) Å (average), respectively) in **4** are very similar to those observed in **3** and related complexes.[9]

Properties. In the solid state, **4** is moderately sensitive to oxygen. The room-temperature (298 K) magnetic susceptibility of polycrystalline **4** (3.23 μ_B) is consistent with a distorted tbp geometry with two unpaired electrons on the Ni(II) center. The complex dissolves in aprotic solvents like DMSO and DMF to give deep reddish brown solutions that are stable for hours in the absence of oxygen. In DMSO, **4** exhibits electronic absorption bands at 1010 nm (ϵ = 50 M^{-1} cm^{-1}), 705 nm (sh, ϵ = 230 M^{-1} cm^{-1}), and 490 nm (ϵ = 13 500 M^{-1} cm^{-1}), which confirms the presence of a pentacoordinated Ni(II) species in solution.[16] The ^1H NMR spectrum of **4** in $(CD_3)_2SO$ is shown in Figure 2. Six isotropically shifted resonances at 176.68, 79.23, 73.43, 50.98, 21.02, and 18.69 ppm (from TMS) are observed for the coordinated terpy ligand. The four meta hydrogens of the two thiolates resonate at 22.63 ppm, while the two para hydrogens give rise to a peak at −21.95 ppm.[9] Area integration indicates that the four methyl groups of the thiolate ligands also resonate at 18.69 ppm along with two terpy hydrogens (Figure 2). That a single nickel complex is present in solution is clear from the clean ^1H NMR spectrum of **4**.

X-ray Absorption Spectroscopic Studies. To date, results of Ni X-ray absorption spectroscopy (XAS) for three [FeNi] hydrogenases have been reported.[7,17-19] In earlier attempts, the data were fitted on the basis of a limited number of model compounds. However, in recent years, the spectra have been reexamined along with a series of Ni(II) and Ni(III) complexes

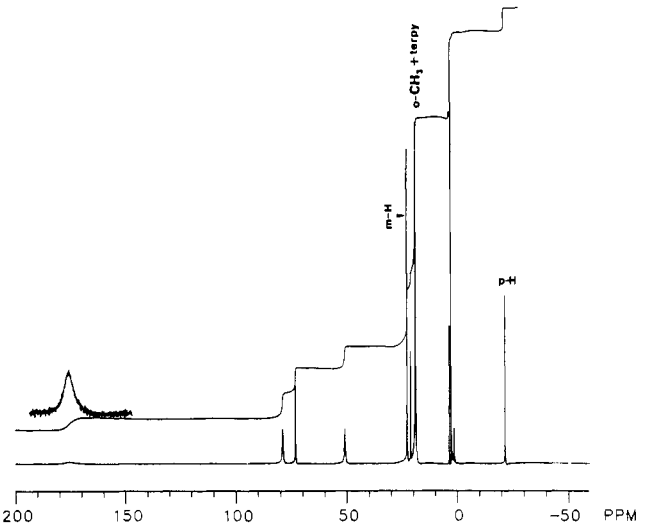

Figure 2. ^1H NMR spectrum (300 MHz, 298 K) of **4** in $(CD_3)_2SO$. Signal assignments for the protons of the thiolate ligands are indicated. The signal from the four CH_3 groups of the thiolate ligands coincides with that of one set of terpy hydrogens.

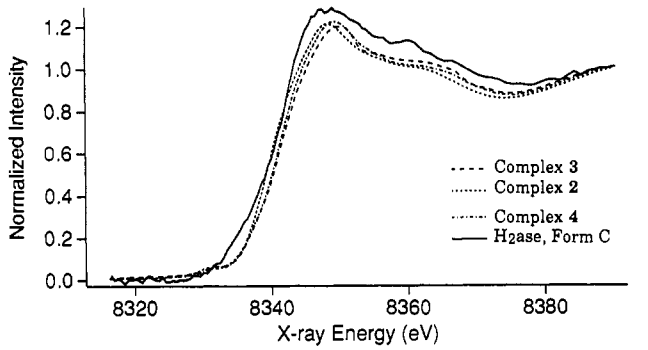

Figure 3. Ni K-edge XANES spectra of complexes **2**–**4** and the hydrogenase (form C) from *T. roseopersicina*.

of varying coordination geometries and with different sets of donor atoms.[7a,b,20] These studies have demonstrated that the features indicated by X-ray absorption near-edge spectroscopy (XANES) are good indicators of the coordination geometry as well as oxidation state(s) of nickel, and at least in the case of the hydrogenase from *T. roseopersicina*, the XAS spectrum is consistent with a distorted tbp geometry and a mixed O/N- and S-donor ligand environment for the biological nickel site. Shown in Figure 3 are the XAS spectra of *T. roseopersicina* hydrogenase (form C) and the model complexes **2**–**4**. The spectra of the model complexes are all very similar to one another. Though crystallographic studies revealed an octahedral structure for **2**,[9] similarities in XAS spectra indicate that the sample of **2** lost the coordinated acetonitrile molecule during sample preparation (and data collection under He) and was converted to a pentacoordinated tbp structure.[21] A weak peak at ~8331 eV assigned to the 1s → 3d transition is observed for all three model complexes. The relative area under this peak is 0.5, which is outside the range (0.09–0.35) observed for hexacoordinated complexes.[7b] The much less pronounced peak at the top of the edge, exhibited by these complexes, is due to the presence of highly polarizable thiolate ligands in the first coordination sphere of the nickel center. Complex **2**, with comparatively harder thiolate ($C_6F_5S^-$) ligands, displays the edge at slightly lower energy with a more pronounced peak compared to **3** and **4**. The four spectra in Figure 3 strongly suggest that complexes **3** and **4** (and **2** without the coordinated

(16) (a) Lever, A. B. P. *Inorganic Electronic Spectroscopy*, 2nd ed.; Elsevier: New York, 1984; pp 520–530. (b) Sacconi, L.; Bertini, I. *J. Am. Chem. Soc.* **1968**, *90*, 5443. (c) Ciampolini, M. *Inorg. Chem.* **1966**, *5*, 35.
(17) Whitehead, J. P.; Colpas, G. J.; Bagyinka, C.; Maroney, M. J. *J. Am. Chem. Soc.* **1991**, *113*, 6288.
(18) (a) Eidsness, M. K.; Sullivan, R. J.; Schwartz, J. R.; Hartzell, P. L.; Wolfe, R. S.; Flank, A.-M.; Cramer, S. P.; Scott, R. A. *J. Am. Chem. Soc.* **1986**, *108*, 3120. (b) Lindahl, P. A.; Kojima, N.; Housinger, R. P.; Fox, J. A.; Teo, B. K.; Walsh, C. T.; Orne-Johnson, W. H. *J. Am. Chem. Soc.* **1984**, *106*, 3062.
(19) Scott, R. A.; Wallin, S. A.; Czechowski, M.; Der Vartanian, D. V.; LeGall, J.; Peck, H. D., Jr.; Moura, I. *J. Am. Chem. Soc.* **1984**, *106*, 6864.
(20) Scott, R. A. *Physica B+C* **1989**, *158*, 84.
(21) Absence of the 1s → 4p_z transition (with shakedown contribution) in the near-edge spectra rules out the possibility of a square pyramidal geometry for the pentacoordinated species.

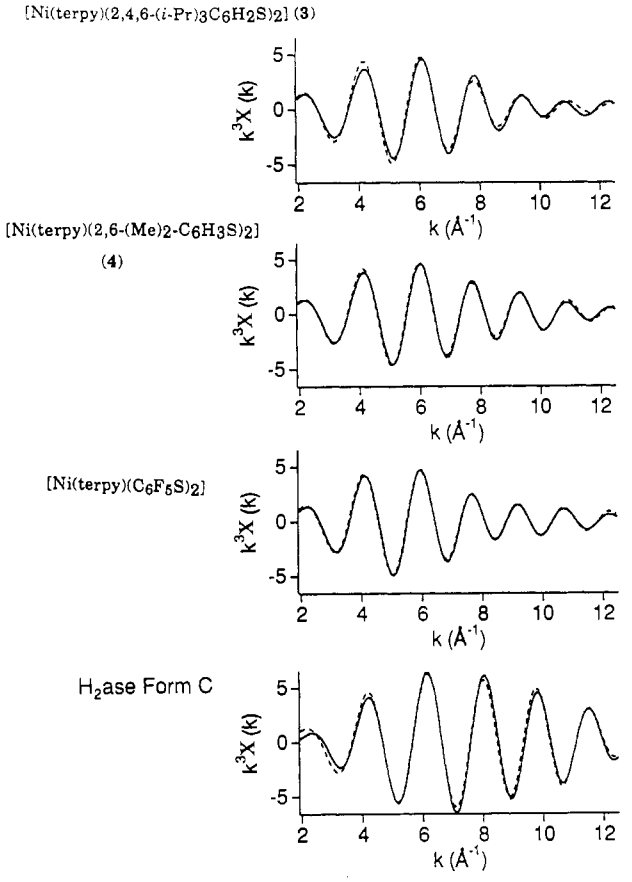

Figure 4. Fourier-filtered Ni K-edge EXAFS spectra (from atoms in the first coordination sphere, back-transform window = 1.1–2.3 Å) of complexes **2–4** and *T. roseopersicina* hydrogenase (form C).

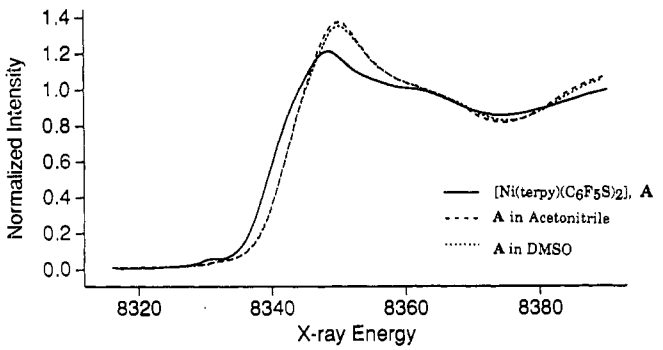

Figure 5. Variation in the Ni XANES spectrum of $[Ni(terpy)(C_6F_5S)_2]$ with different sixth ligands.

acetonitrile molecule) are good structural models for the nickel site in *T. roseopersicina* hydrogenase. Since the XANES data were collected on form C of the hydrogenase, the biological nickel site might contain a H^- ligand at a sixth site in the first coordination sphere (vide infra); this may explain the weak 1s → 3d transition in the near-edge region (Figure 3).

The Fourier-filtered Ni K-edge EXAFS spectra of complexes **2–4** and the hydrogenase from *T. roseopersicina* (form C) are shown in Figure 4. The EXAFS data are summarized in Table IV. In case of the enzyme, the best fit (shown in dashed lines) includes three Ni–N distances of 2.06 (2) Å and two Ni–S distances of 2.21 (2) Å.[7a] For model complexes, interatomic distances obtained from the best fits agree well with those determined by X-ray crystallography (Table IV). It is quite clear from Figure 4 that the spectra obtained for the model complexes **2–4** are similar to that of the enzyme with a maximum at k = 6 $Å^{-1}$. The EXAFS spectra of the model complexes damp out a little faster however. This might result from small differences in bond lengths (Table IV) although the data for the enzyme are

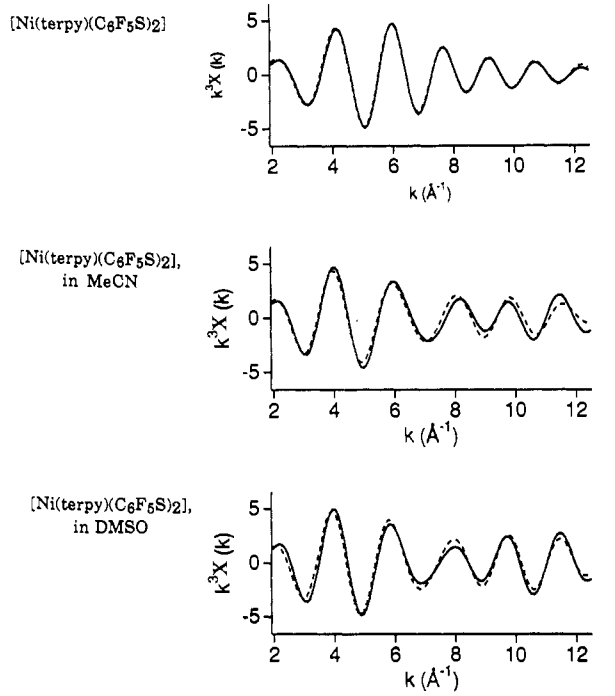

Figure 6. Fourier-filtered Ni K-edge EXAFS spectra of $[Ni(terpy)(C_6F_5S)_2]$ with different sixth ligands (back-transform window 1.1–2.3 Å).

considerably more noisy. The EXAFS spectrum of the enzyme has been previously analyzed on the basis of a number of model complexes containing various sets of donor atoms.[7a] The present results (Figure 4, Table IV) provide strong support for the previous conclusion and also indicate that in form C of *T. roseopersicina* hydrogenase, the coordination geometry around the nickel center is distorted octahedral with three N/O- and two S-donor atoms in a distorted tbp arrangement (H^- or H_2 is the sixth ligand). The EXAFS spectrum of the hydrogenase appears similar to the EXAFS spectrum of the pentacoordinated complexes presumably due to the small backscattering cross section of the H atom(s).

The differences in the XAS spectra for five- and six-coordinated complexes with similar ligand environments are shown in Figures 5 and 6. Shown in Figure 5 are the nickel K-edge XANES spectra of $[Ni(terpy)(C_6F_5S)_2]$ and the same complex in acetonitrile and DMSO solutions. The EXAFS spectra of the same three samples are shown in Figure 6. Since a molecule of acetonitrile is coordinated to nickel in crystals of the less crowded model complex **2** (crystals grown from solution in acetonitrile), the spectra of $[Ni(terpy)(C_6F_5S)_2]$ in acetonitrile and DMSO are in fact the spectra of the hexacoordinated species $[Ni(terpy)(C_6F_5S)_2(solv)]$ (solv = acetonitrile, DMSO). As seen in Figure 5, the hexacoordinated species exhibit very different XANES spectra. First, the 1s → 3d pre-edge peak is much smaller compared to that of the pentacoordinated complex. Second, the more intense peaks of the hexacoordinated species are shifted to higher energy due to the addition of a "hard" N (for acetonitrile) or O (for DMSO) donor atom to the sixth site on nickel. The EXAFS features of the hexacoordinated complexes are also different. Unlike the pentacoordinated complexes, which show maxima at k = 6 $Å^{-1}$ (Figure 4), the hexacoordinated species exhibit maxima at k = 4 $Å^{-1}$. Also, the bond lengths are longer in the acetonitrile and DMSO adducts, which is expected for the change in coordination number from 5 to 6. These results are consistent with the ligand environment of the nickel site in *T. roseopersicina* hydrogenase (form C), which is composed of five non-hydrogen donors in a distorted tbp geometry.

Binding Studies at the Ni(I) Center. Reduction of **4** generates a reduced species **5**, which gives an axial EPR signal (g_1 = 2.249, g_2 = 2.126) (Figure 7A). This is typical for a Ni(I) d^9 system

Table IV. Summary of EXAFS Results for the Model Complexes and the Enzyme

complexes/enzyme	bond distances (EXAFS), Å		$10^3\Delta\sigma^2$, Å^2 [a]	correlations (>0.6)	R[b]	bond distances[c] (crystallographic), Å	
[Ni(terpy)(2,4,6-(*i*-Pr)$_3$C$_6$H$_2$S)$_2$]	3 Ni–N	2.018 (3)	0.8		0.31	3 Ni–N	2.057 (7)
	2 Ni–S	2.283 (2)	2.0			2 Ni–S	2.302 (3)
[Ni(terpy)(2,6-(Me)$_2$C$_6$H$_3$S)$_2$]	3 Ni–N	2.038 (2)	3.7	r_S/σ_N = –0.64	0.14	3 Ni–N	2.044 (3)
	2 Ni–S	2.296 (8)	0.1			2 Ni–S	2.311 (1)
[Ni(terpy)(C$_6$F$_5$S)$_2$]	3 Ni–N	2.026 (1)	1.4		0.10		
	2 Ni–S	2.315 (1)	0.7				
[Ni(terpy)(C$_6$F$_5$S)$_2$]	4 Ni–N	2.060 (3)	–1.4		0.54	4 Ni–N	2.050 (7)
in acetonitrile	2 Ni–S	2.394 (9)	16.3			2 Ni–S	2.491 (4)
[Ni(terpy)(C$_6$F$_5$S)$_2$]	4 Ni–N	2.086 (2)	–3.8		0.46		
in DMSO	2 Ni–S	2.418 (5)	9.6				
T. roseopersicina hydrogenase	3 Ni–N	2.053 (3)	–4.5	r_S/σ_N = –0.77	0.40		
(form C)	2 Ni–S	2.215 (3)	1.0	σ_S/σ_N = –0.67			

[a] $\Delta\sigma^2 = \sigma^2(\text{fit}) - \sigma^2(\text{model})$. [b] $R = [\sum k^6(\chi_c - \chi)^2/n]^{1/2}$. [c] Average bond distances.

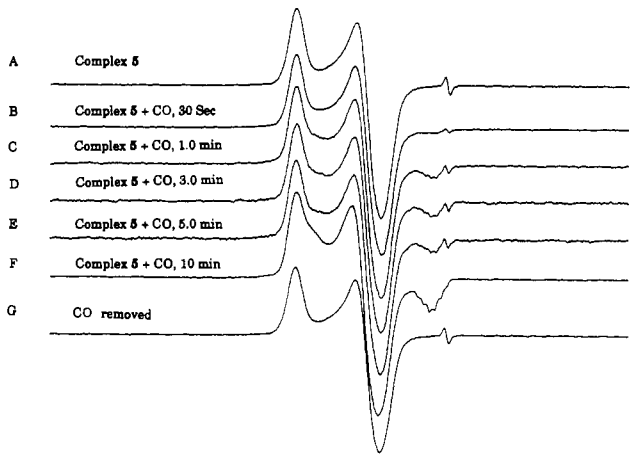

Figure 7. X-band EPR spectra (100 K, DMF glass) of [Ni(terpy)(2,6-(Me)$_2$C$_6$H$_3$S)$_2$]$^-$ (**5**) (trace A) and the CO adduct [Ni(terpy)(2,6-(Me)$_2$C$_6$H$_3$S)$_2$(CO)]$^-$ (**6**) (trace F). Traces B–E show the changes in the EPR spectrum as more and more CO adduct was formed. The spectrum at the bottom (trace G) was obtained when N_2 was passed through the solution of **6** (trace F) at 233 K for 5 min. Spectrometer settings: microwave frequency, 9.43 GHz; microwave power, 10 mW; modulation frequency, 100 kHz; modulation amplitude, 2 G.

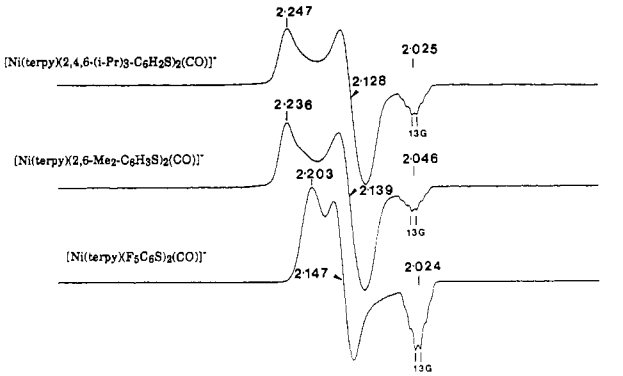

Figure 8. X-Band EPR spectra (100 K) of the CO adducts **6**–**8** in DMF. Selected g and A values are indicated. Spectrometer settings were same as for Figure 7.

with the unpaired electron in the $d_{x^2-y^2}$ orbital.[22] When CO gas is passed through a solution of the reduced species, the CO adduct [Ni(terpy)(2,6-(Me)$_2$C$_6$H$_3$S)$_2$(CO)]$^-$ (**6**) is obtained. Complex **6** exhibits a rhombic signal (g_1 = 2.236, g_2 = 2.139, g_3 = 2.046) with hyperfine splitting in the g_3 region (A = 13 G) (Figure 8B). The CO adduct is quite stable and can be stored for hours at 257 K. Figure 7B–F shows the gradual formation of the CO adduct of complex **5**. When nitrogen gas was passed through the solution of **6** at 237 K, species **5** was regenerated (Figure 7G). These results indicate that CO binding to the nickel center of the reduced species **5** is reversible. Reversible CO binding to the nickel center of [Ni(terpy)(2,4,6-(*i*-Pr)$_3$C$_6$H$_2$S)$_2$(CO)]$^-$ (**7**, the CO adduct of reduced **3**) has been reported in our earlier account.[9] It is evident that the structures of **3** and **4** allow CO to bind to the Ni(I) centers of the corresponding reduced species. The reversibility of the CO-binding reaction in case of **6** and **7** indicates weak binding of CO to the Ni(I) centers in these crowded molecules.

As discussed earlier, complex **2** contains a labile solvent (CH_3CN) molecule as the sixth ligand on nickel. The reduced species from this complex also gives rise to a CO adduct with similar EPR parameters (Figure 8C). It is therefore evident that CO replaces the solvent molecule in the reduced species and gives rise to [Ni(terpy)(C$_6$F$_5$S)$_2$(CO)]$^-$ (**8**) as the sole product. This CO adduct is quite stable and does not lose CO as easily as **6** or **7**. Clearly, less crowding in **8** is one reason that CO binds strongly to the nickel center in this species.

The EPR spectra of the hydride adducts [Ni(terpy)(2,6-(Me)$_2$C$_6$H$_3$S)$_2$(H$^-$)]$^{2-}$ (**9**) and [Ni(terpy)(2,4,6-(*i*-Pr)$_3$C$_6$H$_2$S)$_2$(H$^-$)]$^{2-}$ (**10**) are shown in the Figure 9. Overall, the EPR spectrum of **10** exhibits a greater extent of rhombicity compared to that of **9**. In both hydride adducts, the unpaired electron occupies the d_{z^2} orbital and interacts with two N (I = 1) nuclei at the axial positions. Therefore, five lines are observed in the g_3 region of **9** and **10**. The hydride adducts are less stable compared to the CO adducts.

EXAFS studies have indicated that the active site of carbon monoxide dehydrogenases (CODH) contains nickel in a coordination environment of sulfur- and nitrogen-donor ligands.[23] It has been suggested that acetate synthesis for the acetyl-CoA process involves coordination of a methyl group to the nickel site of CODH.[24] We, therefore, have investigated the possibility of binding of alkyl groups to nickel in the reduced forms of complexes **3** and **4**. Addition of lithium alkyls (LiR, R = CH_3, $CH_3(CH_2)_2$-CH_2) in THF to solutions of **3** and **4** in DMF at ~240 K affords the desired alkyl adducts. The EPR spectra are shown in Figure 10. LiR also serves as the reductant in these reactions. These spectra are very similar to those of the hydride adducts (Figure 9). This fact prompted us to formulate the alkyl adducts as [Ni(terpy)(SR)$_2$(R$^-$)]$^{2-}$. The alkyl radicals, generated in the above-mentioned reaction, produce EPR signals centered at g =

(22) (a) Lappin, A. G.; McAuley, A. *Adv. Inorg. Chem.* **1988**, *32*, 241. (b) Salerno, J. C. In *The Bioinorganic Chemistry of Nickel*; Lancaster, J. R., Jr., Ed.; VCH Publishers: Deerfield Beach, FL, 1988; Chapter 3, p 53. (c) Nag, K.; Chakravorty, A. *Coord. Chem. Rev.* **1980**, *33*, 87.

(23) (a) Ragsdale, S. W.; Wood, H. G.; Morton, T. A.; Ljungdahl, L. G.; Der Vantanian, D. V. In *The Bioinorganic Chemistry of Nickel*; Lancaster, J. R., Jr., Ed.; VCH Publishers: Deerfield Beach, FL, 1988; Chapter 14, p 311. (b) Bastian, N. R.; Diekert, G.; Niederhoffer, E. C.; Teo, B.-K.; Walsh, C. T.; Orme-Johnson, W. H. *J. Am. Chem. Soc.* **1988**, *110*, 5581. (c) Cramer, S. P.; Eidsness, M. K.; Pan, W.-H.; Morton, T. A.; Ragsdale, S. W.; Der Vartanian, D. V.; Ljungdahl, L. G.; Scott, R. A. *Inorg. Chem.* **1987**, *26*, 2477.

(24) (a) Pezacka, E.; Wood, H. G. *J. Biol. Chem.* **1986**, *261*, 1609. (b) Ragsdale, S. W.; Wood, H. G. *J. Biol. Chem.* **1985**, *260*, 3970.

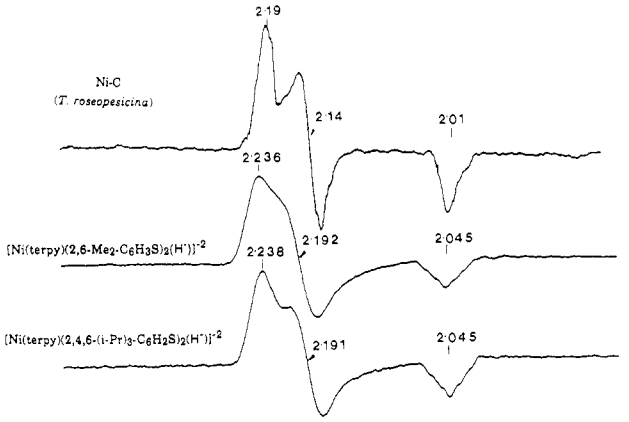

Figure 9. X-Band EPR spectra (100 K) of *T. roseopersicina* hydrogenase (form C, top trace) and the two hydride adducts **9** and **10**. Selected g values are indicated. Spectrometer settings were the same as for Figure 7.

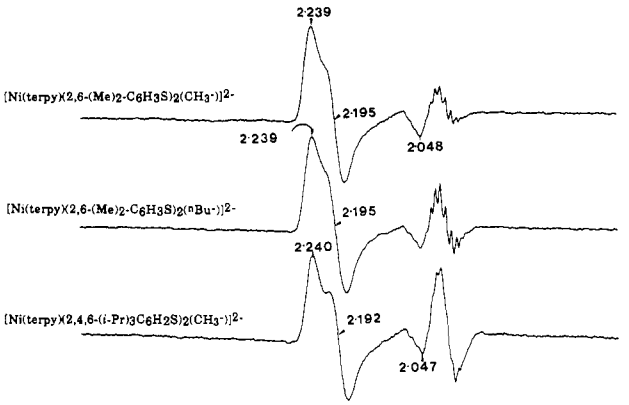

Figure 10. X-Band EPR spectra (100 K) of the alkyl adducts $[Ni(terpy)(SAr)_2(R^-)]^{2-}$. Top trace: Ar = 2,6-$(Me)_2C_6H_3$, R = CH_3. Middle trace: Ar = 2,6-$(Me)_2C_6H_3$, R = n-Bu. Bottom trace: Ar = 2,4,6-$(i\text{-}Pr)_3C_6H_2$, R = CH_3. Selected g values are indicated. For spectrometer settings, see the caption to Figure 7.

Scheme I

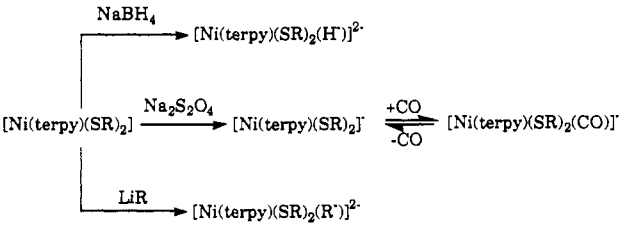

2.00 (Figure 10). The intensity of the alkyl signal diminishes as the sample solution is warmed to 250–260 K. When stored at 253 K, these alkyl adducts are stable for several hours.

The mechanism of CODH involves insertion of CO into the Ni–alkyl bond to form the acetyl group that eventually leads to the formation of acetyl-CoA. This insertion step requires both CH_3 and CO groups to be coordinated to the nickel site of the enzyme.[23a,24] In the present study, all attempts to insert CO into the Ni–alkyl bond in $[Ni(terpy)(SR)_2(R^-)]^{2-}$, however, failed. We attribute this failure to the lack of a temporary CO-binding site in the coordinatively saturated Ni(I) complexes, $[Ni(terpy)(SR)_2(R^-)]^{2-}$. Scheme I summarizes the reactions of the pentacoordinated model complexes.

Distinct differences in the EPR signals of the reduced and substrate-bound species imply electronic reorganization at the nickel center upon substrate binding. In the reduced state, the unpaired electron presumably resides in the $d_{x^2-y^2}$ orbital.[22] Binding of H^- to the reduced nickel center takes place at the sixth site. The substrate-bound species acquire a distorted octahedral geometry, and the binding perturbs the crystal field splitting pattern and raises the energy of d_{z^2} over that of $d_{x^2-y^2}$. As a consequence, the unpaired electron moves to the d_{z^2} orbital, couples with two N nuclei at the axial positions, and gives rise to the five-line hyperfine splitting pattern in the g_3 region (Figure 9).

Distortions due to steric constraints around the nickel center of the adducts appear to affect the rhombicity observed in their EPR spectra. As shown in Figure 8, the less hindered complex $[Ni(terpy)(C_6F_5S)_2(CO)]^-$ exhibits a less rhombic signal compared to the more crowded complex **6** and **7**. Similar trends are also observed with the hydride and alkyl adducts. The higher rhombicity noted in the signals of the biological nickel site presumably indicates a highly distorted nickel center.[25]

Comparison with the Ni Site in Hydrogenase

The oxidized forms (as isolated) of [FeNi] hydrogenases from different microorganisms are EPR active, and the nickel center exhibits two rhombic signals termed Ni-A (g_1 = 2.31, g_2 = 2.23, g_3 = 2.02) and Ni-B (g_1 = 2.33, g_2 = 2.16, g_3 = 2.02). Both of these signals are assigned to formally Ni(III) species. Upon reduction by hydrogen, both the signals disappear and a new rhombic signal (g_1 = 2.19, g_2 = 2.14, g_3 = 2.02) termed Ni–C (form C in our work) is detected. The Ni-A and Ni-B signals reappear upon oxidation in relative ratios that are dependent on the method of oxidation.[1b,c,31a] Almost all hydrogenases are inhibited by carbon monoxide.[26–28] This inhibition, in most cases, is competitive with hydrogen binding. EPR studies on CO binding to the [FeNi] hydrogenases demonstrate that CO binds to the nickel center.[6,29] When carbon monoxide is passed through solutions containing the enzyme in the reduced form, the Ni-C signal slowly disappears and a new rhombic signal is observed. The intensity of the new rhombic signal reaches its maximum only after repeated evacuation and flushing with CO.[6a] In the present study, similar behavior is observed for complexes **3** and **4**. In their reduced states, both complexes bind CO and produce rhombic EPR signals whose intensities progressively increase with repeated purging with CO (Figure 7A–F). As with the enzyme, binding of CO to the Ni(I) centers of these complexes is also reversible (Figure 7G).

Studies on hydrogenases suggest that the Ni-A and Ni-B signals represent the oxidatively deactivated and catalytically inactive forms of the enzyme.[30,31] Some of the [FeNi] hydrogenases do not exhibit these signals.[32] In contrast, all [FeNi] hydrogenases exhibit the Ni-C signal. This Ni-C signal presumably arises from a key intermediate species formed in the catalytic process.[31b,33] Kinetic studies[34,35] on hydrogen activation by hydrogenases

(25) Less polar solvents also lower the rhombicity of these EPR signals.
(26) Berlier, Y.; Fauque, G. D.; LeGall, J.; Choi, E. S.; Peck, H. D., Jr.; Lespinat, P. A. *Biochem. Biophys. Res. Commun.* **1987**, *146*, 147.
(27) Serra, J. L.; Llama, M. J.; Hall, D. O. *Arch. Biochem. Biophys.* **1984**, *234*, 73.
(28) Heerikhuizen, H. V.; Albracht, S. P. J.; Slater, E. C.; van Rheenen, P. S. *Biochim. Biophys. Acta* **1981**, *657*, 26.
(29) Der Vartanian, D. V.; Kruger, H. J.; Peck, H. D., Jr.; LeGall, J. *Rev. Port. Quim.* **1985**, *27*, 70.
(30) Teixeira, M.; Moura, I.; Xavier, A. V.; Huynh, B. H.; Der Vartanian, D. V.; Peck, H. D., Jr.; LeGall, J.; Moura, J. J. G. *J. Biol. Chem.* **1985**, *260*, 8942.
(31) (a) Cammack, R.; Fernandez, V. M.; Schneider, K. In *Bioinorganic Chemistry of Nickel*; Lancaster, J. R., Jr.; Ed.; VCH Publishers: Deerfield Beach, FL, 1988; Chapter 8, p 167. (b) Fernandez, V. M.; Hatchikian, E. C.; Cammack, R. *Biochim. Biophys. Acta* **1985**, *832*, 69.
(32) (a) Teixeira, M.; Fauque, G.; Moura, I.; Lespinat, P. A.; Berlier, Y.; Prickril, B.; Peck, H. D., Jr.; Xavier, A. V.; LeGall, J.; Moura, J. J. G. *Eur. J. Biochem.* **1987**, *167*, 47. (b) Teixeira, M.; Moura, I.; Fauque, G.; Czechowski, M.; Berlier, Y.; Lespinat, P. A.; LeGall, J.; Xavier, A. V.; Moura, J. J. G. *Biochimie* **1986**, 75.
(33) (a) Fan, C.; Teixeira, M.; Moura, J. J. G.; Moura, I.; Huynh, B.-H.; LeGall, J.; Peck, H. D., Jr.; Hoffman, B. M. *J. Am. Chem. Soc.* **1991**, *113*, 20. (b) Cammack, R.; Patil, D.; Fernandez, V. M. *Biochem. Soc. Trans.* **1985**, *13*, 572.
(34) Krasna, A. I.; Rittenberg, D. *J. Am. Chem. Soc.* **1954**, *76*, 3015.
(35) Fauque, G. D.; Berlier, J. M.; Czechowski, M. H.; Dimon, B.; Lespinat, P. A.; LeGall, J. *J. Ind. Microbiol.* **1987**, *1*, 1.

Table V. Spectroscopic Data

$[Ni(terpy)(2,6\text{-}Me)_2C_6H_3S)_2]$ (**4**)

electronic absorption data (solvent DMSO; λ_{max}, nm (ϵ, M^{-1} cm^{-1})): 1010 (50), 705 (230), 490 (sh, 13 500), 324 (sh, 46 000), 284 (67 600)

^1H NMR data (solvent $(CD_3)_2SO$; 298 K; δ (ppm) from TMS): 176.68, 79.23, 73.43, 50.98, 22.63, 21.02, 18.69, -21.95

EPR Data (DMF Glass; 100 K)

complexes/enzymes (form C)	g (A, G)
$[Ni(terpy)(2,6\text{-}(Me)_2C_6H_3S)_2]^-$	2.249, 2.126
$[Ni(terpy)(2,4,6\text{-}(i\text{-}Pr)_3C_6H_2S)_2]^-$	2.247, 2.123
$[Ni(terpy)(2,6\text{-}(Me)_2C_6H_3S)_2(CO)]^-$	2.236, 2.139, 2.046 (13)
$[Ni(terpy)(2,4,6\text{-}(i\text{-}Pr)_3C_6H_2S)_2(CO)]^-$	2.247, 2.128, 2.025 (13)
$[Ni(terpy)(2,6\text{-}(Me)_2C_6H_3S)_2(H^-)]^{2-}$	2.236, 2.192, 2.045
$[Ni(terpy)(2,4,6\text{-}(i\text{-}Pr)_3C_6H_2S)_2(H^-)]^{2-}$	2.238, 2.191, 2.045
T. rosepersicina[37]	2.19, 2.14, 2.01
Desulfivibrio gigas[30]	2.19, 2.14, 2.02
Mb. thermoautotrophicum[40]	2.196, 2.140, 2.00
Desulfovibrio baculatus[41]	2.20, 2.16, 2.00
$[Ni(terpy)(2,6\text{-}(Me)_2C_6H_3S)_2(CH_3^-)]^{2-}$	2.239, 2.195, 2.048
$[Ni(terpy)(2,4,6\text{-}(i\text{-}Pr)_3C_6H_2S)_2(CH_3^-)]^{2-}$	2.240, 2.192, 2.047
$[Ni(terpy)(2,6\text{-}(Me)_2C_6H_3S)_2(n\text{-}Bu^-)]^{2-}$	2.239, 2.195, 2.049

indicate that the process involves heterolytic cleavage of H_2 with the possible formation of a metal hydride (M–H^-) species as an intermediate. This idea has been supported by photolysis studies on the reduced enzyme[6b,36] as well as by ^1H and ^2H Q-band ENDOR experiments.[33a] Shown in Figure 9 are the EPR spectra of the hydrogenase (form C) from *T. roseopersicina* and the hydride adducts of the reduced forms of **3** and **4**. The enzyme exhibits a rhombic signal with $g_1 = 2.19$, $g_2 = 2.14$, and $g_3 = 2.01$ (Figure 9A). The EPR spectra of the hydride adducts **9** and **10** are also rhombic (Figure 9B,C). The similarities in shape and g values among these spectra are especially noticeable. Ni-C species obtained from other [FeNi] hydrogenases also exhibit rhombic signals with g values similar to those of the model complexes (Table V). Collectively, the spectra in Figure 9 indicate that a Ni(I)–H^- intermediate could be responsible for the Ni-C signal.[2b]

It has also been postulated that the Ni-C signal could arise from a Ni(III) species.[1d,30] The presence of a Ni(III) center in the reduced form (form C) of the enzyme, however, is inconsistent with the results of the CO/H^- binding studies on the enzymes as well as the model systems. Carbon monoxide does not bind to the oxidized form (Ni-A/Ni-B) of the enzyme, where nickel is likely to be in +3 oxidation state.[6a,29] Photolysis studies indicate that CO and H^- bind to the same site in the reduced enzyme, which is also consistent with the competitive inhibition of hydrogenases by CO. Carbon monoxide is a very good π-acid ligand and hence strongly binds to metals in low oxidation states.[38] A large number of Ni(0) and Ni(I) carbon monoxide complexes have been characterized.[22c,39] In contrast, no Ni(III)–CO complex has been reported so far. It is quite unlikely that CO binding to the reduced enzyme takes place at a nickel site which is in the +3 oxidation state.

In the present work, binding studies have been performed on Ni(I) complexes. The spectral data are very similar to those obtained from the hydride or carbon monoxide adducts of the enzyme in the reduced form. This work, therefore, supports the existence of Ni(I)–H^- species in form C of [FeNi] hydrogenases.

Summary and Conclusion

The following are the principal results and conclusion of this investigation.

(1) The distorted trigonal bipyramidal (tbp) complex $[Ni(terpy)(2,6\text{-}(Me)_2C_6H_3S)_2]$ (**4**) has been isolated from the reaction of $[Ni(terpy)Cl_2]$ with $2,6\text{-}(Me)_2C_6H_3S^-$. The structure of **4** has been determined by X-ray crystallography. Similar synthetic strategy had also afforded the other tbp complex $[Ni(terpy)(2,4,6\text{-}(i\text{-}Pr)_3C_6H_2S)_2]$ (**3**) reported in an earlier account.

(2) The complexes **3** and **4** (and **2** without the coordinated acetonitrile molecule) are very good structural models for the nickel site of *T. roseopersicina*, since the XAS data for the enzyme indicate that a tbp geometry with 2 ± 1 $S(Cl)^-$ donor atoms at an average distance of 2.22 (2) Å and 3 ± 1 N/O-donor atoms at an average distance of 2.05 (2) Å is the best description of the biological nickel site.

(3) The model complexes **2**–**4** are easily reduced to the corresponding Ni(I) species with reductants like dithionite in DMF and other solvents.

(4) CO binds to the Ni(I) centers of the reduced model complexes $[Ni(terpy)(SR)_2]^-$ in a reversible manner.

(5) The EPR spectra of the CO adducts $[Ni(terpy)(RS)_2(CO)]^-$ and the H^- adducts $[Ni(terpy)(RS)_2(H^-)]^{2-}$ resemble those obtained for the enzyme rather closely. Similarities clearly indicate the presence of Ni(I) in the reduced form of the enzyme.

(6) Though alkyl groups bind to the Ni(I) centers of the reduced model complexes (EPR data), all attempts to insert CO into the M–alkyl bonds have failed. This failure is attributed to the lack of a temporary CO-binding site on Ni(I) in the alkyl adducts of the model complexes. In other words, this result indicates that there exist at least two binding sites on nickel in CODH for transient binding of both the alkyl and CO ligands before the formation of the acetyl group at the active site.

Acknowledgment. Financial support of grants from the Petroleum Research Fund, administered by the American Chemical Society (to P.K.M.), and from the NIH (GM-38829, to M.J.M.) is gratefully acknowledged.

Supplementary Material Available: A drawing of complex **4** showing the planarity of the terpy ligand (Figure S1) and crystal structure data for **4**, including anisotropic displacement coefficients (Table S1) and H atom coordinates (Table S2) (2 pages); a listing of observed and calculated structure factors (Table S3) (9 pages). Ordering information is given on any current masthead page.

(36) Cammack, R.; Patil, D. S.; Hatchikian, E. C.; Fernandez, V. M. *Biochim. Biophys. Acta* **1987**, *912*, 98.

(37) Cammack, R.; Bagyinka, C.; Kovacs, K. L. *Eur. J. Biochem.* **1989**, *182*, 357.

(38) (a) Malatesta, L.; Cenini, S. *Zerovalent Compounds of Metals*; Academic: London, 1974. (b) Ugo, R. *Coord. Chem. Rev.* **1968**, *3*, 319. (c) Nyholm, R. S.; Tobe, M. L. *Adv. Inorg. Chem. Radiochem.* **1963**, *5*, 1. (d) Orgel, L. E. *An Introduction to Transition Metal Chemistry*; Methuen: London, 1960.

(39) Sacconi, L.; Mani, F.; Bencini, A. In *Comprehensive Coordination Chemistry*; Wilkinson, G., Ed.; Pergamon Press: London, 1987; Vol. 5, p 1.

(40) Kojima, N.; Fox, J.; Hausinger, R.; Daniels, L.; Orme-Johnson, W. H.; Walsh, C. T. *Proc. Natl. Acad. Sci. U.S.A.* **1983**, *80*, 378.

(41) Teixeira, M.; Moura, I.; Xavier, A. V.; Moura, J. J. G.; Fauque, G.; Pickrill, B.; LeGall, J. *Rev. Port. Quim.* **1985**, *27*, 194.